Steric and Electronic Effects of Carbene Substitution in Grubbs First-Generation Catalysts

David R. Lane, Christine M. Beavers, Marilyn M. Olmstead, and Neil E. Schore*

Department of Chemistry, University of California, Davis, California 95616

Received August 31, 2009

The relative energies of the carbene species in a variety of metathesis reactions catalyzed by Grubbs first-generation catalyst $(Cy_3P)_2Cl_2Ru{=}CHC_6H_5$ have been determined. High-quality equilibrium data are obtainable by ^1H NMR methods. In the case of *para*-substituted aromatic derivatives $(Cy_3P)_2Cl_2Ru{=}CH(p\text{-}C_6H_4X)$, the carbenes are stabilized by donor substituents, and energies may be determined indirectly by use of either NMR data or Hammett correlations, because only electronic effects are operative. Four systems have been characterized by X-ray crystallography. The energies of alkyl-substituted carbenes $(Cy_3P)_2Cl_2Ru{=}CHR$ are almost entirely dependent on steric interactions.

Introduction

During the course of an olefin metathesis reaction catalyzed by typical ruthenium-based catalysts, there is no single catalyst species *per se*. Instead, the "catalyst" partitions into a family of closely related metal complexes by the process of carbene exchange.[1−4] Equation 1 presents the overall process, the exchange of two diphosphine precatalyst species.

$$(Cy_3P)_2Cl_2Ru{=}\!\!\!\bigvee_{Ph} + \bigvee_{^nBu} \underset{k_r}{\overset{k_f}{\rightleftharpoons}} (Cy_3P)_2Cl_2Ru{=}\!\!\!\bigvee_{^nBu} + \bigvee_{Ph} \quad (1)$$

$$\mathbf{1} \qquad\qquad\qquad\qquad \mathbf{2}$$

Mechanistically, the first step is the dissociation of phosphine from the initial complex **1**, governed by unimolecular rate constant k_1, to give an activated 14-electron monophosphine complex. This step is followed by association with an alkene, governed by bimolecular rate constant k_2, which rapidly leads to the metallacyclobutane intermediate. Subsequent ring-opening and alkene dissociation followed by reassociation of phosphine gives the second resting state diphosphine carbene complex **2** (Scheme 1).[5−7] The diphosphine complexes at the end points of the exchange reaction are readily detectable by conventional NMR spectroscopy, whereas the activated monophosphine complexes typically are not.

The kinetics of carbene exchange of a Grubbs first-generation (G1) catalyst to form either Schrock[4,5,8] or Fischer[7,9] carbenes has been examined by Grubbs using ^1H NMR spectroscopy. The exchange reaction is rapid in C_6D_6, but good kinetic data were obtained by cooling to 7 °C. Phosphine exchange experiments by Grubbs[4,6] established that in G1 complexes the rate constant k_{-1} for recombination of monophosphine intermediates with phosphine is anywhere from 2 to 4 orders of magnitude larger than k_2. Thus, the rates of carbene exchange measured by Grubbs refer to carbene exchange by the active monophosphine carbene intermediates rather than between the observed resting state diphosphine complexes.

We were interested in complementing these studies by investigation of this exchange reaction as a function of alkene structure from a thermodynamic point of view. We are aware of only two instances to date in which carbene equilibration in olefin metathesis catalysts has been mentioned in the literature, and then only as brief asides.[4,8] Data on equilibrium constants for carbene exchange are correspondingly sparse. The forward and reverse rate constants k_f and k_b reported[8] for Grubbs G1 benzylidene **1** with 1-hexene (eq 11) allow derivation of the equilibrium constant for this exchange reaction between the benzylidene and pentylidene **2** as 0.19 for the *mono*phosphine intermediates. We are unaware of any published equilibrium constants for carbene exchange between first-generation diphosphine complexes. Thus we set out to develop a simple system that would enable us to measure these processes.

Results and Discussion

Preliminary Results and Experimental Design. Using ^1H NMR integration data of the carbene protons, we measured the relative concentrations vs time of the benzylidene (**1**, ♦, signal at δ 20.62), pentylidene (**2**, ■, δ 19.80), and methylidene (**3**, ▲, δ 19.41) complexes upon treatment of a solution

*Corresponding author. E-mail: schore@chem.ucdavis.edu.
(1) Herisson, J.-L.; Chauvin, Y. *Makromol. Chem.* **1971**, *141*, 161–176.
(2) Nguyen, S. T.; Johnson, L. K.; Grubbs, R. H. *J. Am. Chem. Soc.* **1992**, *114*, 3974–75.
(3) Nguyen, S. T.; Grubbs, R. H. *J. Am. Chem. Soc.* **1993**, *115*, 9858–59.
(4) Schwab, P.; Grubbs, R. H.; Ziller, J. W. *J. Am. Chem. Soc.* **1996**, *118*, 100–110.
(5) Dias, E. L.; Nguyen, S.-B. T.; Grubbs, R. H. *J. Am. Chem. Soc.* **1997**, *119*, 3887–3897.
(6) Sanford, M.; Ulman, M.; Grubbs, R. H. *J. Am. Chem. Soc.* **2001**, *123*, 749–50.
(7) Sanford, M. S.; Love, J. A.; Grubbs, R. H. *J. Am. Chem. Soc.* **2001**, *123*, 6543–6554.

(8) Ulman, M.; Grubbs, R. H. *Organometallics* **1998**, *17*, 2484–2489.
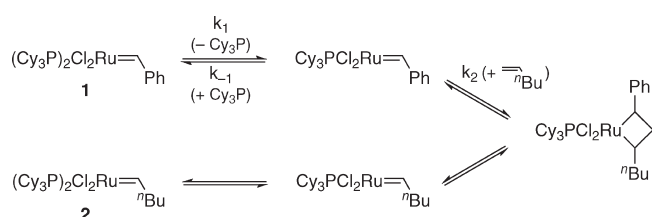(9) Louie, J.; Grubbs, R. H. *Organometallics* **2002**, *21*, 2153–2164.

Figure 1. Carbene speciation vs time for a Grubbs first-generation catalyst reacting with a 20-fold excess of 1-hexene in benzene at room temperature.
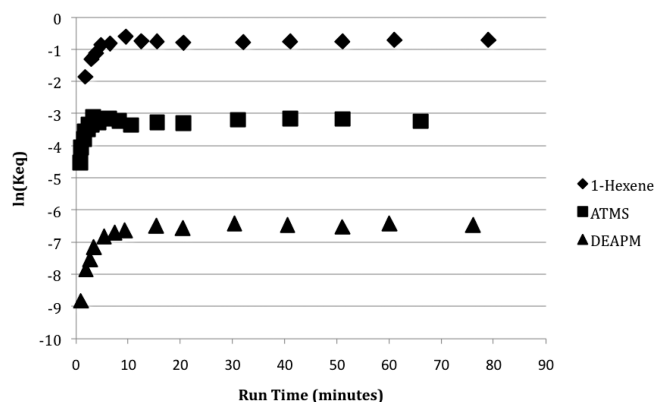
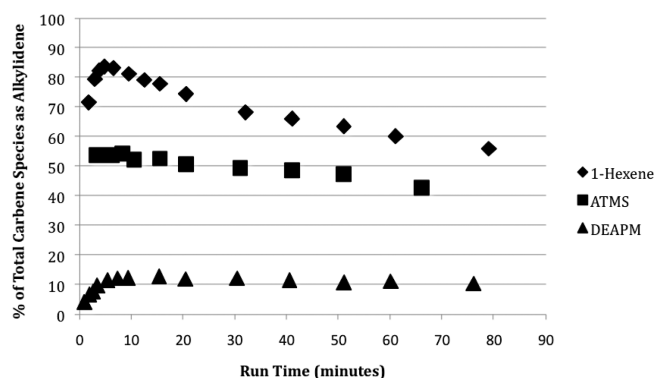**Scheme 1. Mechanistic Detail of Carbene Exchange in a Grubbs G1 Catalyst**


Figure 2. $\ln(K_{eq})$ vs time for Grubbs first-generation catalyst reacting with 1-hexene, ATMS, and DEAPM. Legend: ♦ = carbene **2**; ■ = **4**; ▲ = **5**.

Figure 3. Percent alkylidene vs time for Grubbs first-generation catalyst reacting with 1-hexene, ATMS, and DEAPM. Legend: ♦ = **2**; ■ = **4**; ▲ = **5**.

of Grubbs first-generation catalyst in C_6D_6 with a 20-fold molar excess of 1-hexene at room temperature. The results are shown in Figure 1. Early in the reaction the concentration of **1** decreases as it is rapidly replaced by **2**. Approximately 5 min after addition of substrate the concentrations of **1** and **2** begin to drop off more slowly and in tandem, as a consequence of the ultimate conversion of 1-hexene (O) to 5-decene and the corresponding accumulation of the methylidene complex **3**.

Intrigued by this, we wondered if carbenes **1** and **2** were in fact establishing equilibrium under these conditions. Evaluation of the hypothetical equilibrium constant $K_{eq} = ([pentylidene\ 2][styrene])/([benzylidene\ 1][1-hexene])$ for each data point in Figure 1 demonstrated that equilibrium had been reached by ~5 min after substrate addition, with $K_{eq} = 0.47 \pm 0.04$ for four runs. No change in total carbene concentration was detected during these experiments.

The bulkier substrates allyltrimethylsilane (ATMS) and diethyl allylpropylmalonate (DEAPM) gave very similar results under identical conditions. The latter was chosen for its structural similarity to diethyl diallylmalonate (DEDAM), a substrate commonly used to test catalysts for ring-closing metathesis activity.[5,10] Reaction of each of these substrates with Grubbs G1 led to carbene equilibration within ~5−10 min. A comparative plot of $\ln(K_{eq})$ vs time for the reaction of **1** with each of these three alkenes is shown in Figure 2. At equilibrium considerably less of alkylidenes **4** and **5** is present compared with **2**, as might be expected due to interaction of their more bulky carbene substituents with the cyclohexyl groups on the phosphine ligands.[8] Figure 3
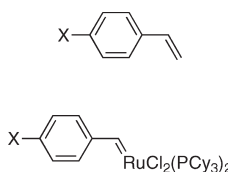
displays the same result in terms of the lower relative concentrations of alkylidenes **4** and **5** in the mixtures.
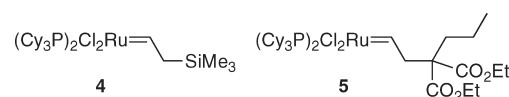
On the basis of these preliminary observations, we undertook a closer examination of carbene equilibration. In order to increase the accuracy of our data, we had to modify our procedure slightly. First, the amount of substrate was reduced from a 20-fold molar excess over the catalyst to a constant $10\,\mu L$ in 0.5 mL of catalyst solution. This resulted in the signals of the substrate and styrene having similar concentrations and made accurate integration of the two signals easier. Second, we modified our NMR protocols to allow collection of better equilibrium data. While in kinetic studies it is preferable to have short interpulse delay times (D2) in order to follow the rapidly changing concentrations of the species under study, we found that this did not give sufficiently accurate results for equilibrium work. We therefore increased delay times in order to obtain more accurate integration data (see Experimental Section for details).[11] In order to avoid excessively large changes in the concentration of species given the long delay times, during acquisition we

(10) Buchowicz, W.; Ingold, F.; Mol, J. C.; Lutz, M.; Spek, A. L. *Chem.−Eur. J.* **2001**, *7*, 2842–2847.

(11) Claridge, T. D. W. *High Resolution NMR Techniques in Organic Chemistry: Tetrahedron Organic Chemistry Series* Vol. *19*; Baldwin, J. E.; Williams, R. M., Series Eds.; Pergamon: New York, 1999.

Table 1. ^{1}H and ^{31}P NMR data (C$_6$D$_6$) for Aromatic Substrates and Complexes

	X =	alkene ^{1}H ppm	carbene ^{1}H ppm	^{31}P ppm
1	OCH$_3$	6.675	20.12	36.062
2	CH$_3$	6.622	20.45	36.556
3	Br	6.338	20.47	36.924
4	Cl	6.365	20.48	36.908
5	H	6.579	20.62	36.702
6	CO$_2$CH$_3$	6.435	20.96	37.298
7	CO$_2$H	6.402	21.03	37.465

Table 2. ^{1}H NMR Data (C$_6$D$_6$) for Aliphatic Substrates and Complexes

	Substrate	Alkene ^{1}H ppm	Carbene ^{1}H ppm	^{31}P ppm
8		5.250	19.406	43.227
9		5.716	19.671	35.868
10	C$_2$	5.793	19.834	36.488
11	C$_3$	5.739	19.802	36.285
12	C$_4$	5.759	19.801	36.078
13	C$_5$	5.774	19.811	36.086
14	C$_6$	5.784	19.820	36.062
15	C$_8$	5.797	19.828	36.078
16		5.749	19.641	36.460
17		5.807	20.411	...
18		5.637	...	...
19		5.722	20.103	35.707
20		5.789	20.563	32.858
21	Si (ATMS)	5.765	19.957	32.041
22	E E H (DEAM)	5.734	19.691	36.921
23	E E (DEAMM)	5.808	20.176	31.586
24	E E (DEAEM)	5.761	20.092	29.001
25	E E (DEAPM)	5.787	20.120	29.085

delayed the data collection for at least one hour after substrate addition in the case of aliphatic substrates and for 20−24 h in the case of aromatic substrates, because the latter required significantly longer to reach equilibrium.

To react with G1 we selected 24 alkenes having a wide range of steric and electronic properties. These consisted of six *para*-substituted styrenes (Table 1) and 18 aliphatic alkenes (eight linear, three branched at carbon 2, three branched at carbon 3, and four allyl malonate esters, Table 2). On the basis of the X-ray crystal structures of the *para*-bromobenzylidene and three other complexes (Figure 4 and *vide infra*), we expected that the *para*-substituents in these complexes would exert only an electronic effect, because these substituents are sufficiently remote from the other ligands as to virtually eliminate any significant steric interaction. In contrast, we expected that the aliphatic substrates would exert primarily a steric effect on the equilibrium, with electronic differences being relatively minor. A discussion of the NMR data in Tables 1 and 2 is forthcoming.

Carbenes with Aromatic Substituents. Carbene exchange reactions of Grubbs G1 with *para*-substituted styrenes were carried out in C$_6$D$_6$ at 20.1−20.3 °C as described above. These processes exhibited equilibrium constants, K_{eq} = ([alkylidene]-[styrene])/([benzylidene][alkene]), ranging from 0.295 ± 0.01 (X = CO$_2$H) to 8.66 ± 0.35 (X = OCH$_3$). Applying the relation $\Delta G = -RT \ln(K_{eq})$ gave the relative Gibbs free energies of the complexes, which ranged from −1.257 kcal/mol (standard deviation 24 cal/mol) to 0.684 kcal/mol (standard deviation 20 cal/mol) relative to the parent benzylidene. The results of these exchange experiments are displayed in Table 3. As expected for an electrophilic metal complex, the more electron-donating substituents gave complexes having lower free energies, while the electron-withdrawing ester and carboxylic acid gave the highest free energies of the substrates tested.

An initial attempt to construct a linear free energy relationship using traditional sigma values ($\sigma_r + \sigma_i$) without parametrization gave a poor correlation with considerable scatter ($R^2 = 0.88$). We therefore turned to the dual parameter method[12,13] in which separate resonance and inductive σ terms specific to a given substituent are multiplied by reaction-specific weighting parameters ρ. The relation used was thus

$\Delta G = m(\rho_r\sigma_r + \rho_i\sigma_i) + b$. We used σ_i and σ_r(BA) parameters given by Ehrenson, Brownlee, and Taft[13] for all substituents except −CO$_2$H. For the latter we used the corresponding σ_i and $\sigma_r°$ Taft scale parameters given by Exner.[14]

(12) Topsom, R. D. *Prog. Phys. Org. Chem.* **1976**, *12*, 1–20.
(13) Ehrenson, S.; Brownlee, R. T. C.; Taft, R. W. *Prog. Phys. Org. Chem.* **1973**, *10*, 1–80.

(14) Exner, O. *Correlation Analysis of Chemical Data*; Plenum Press: New York, 1988.
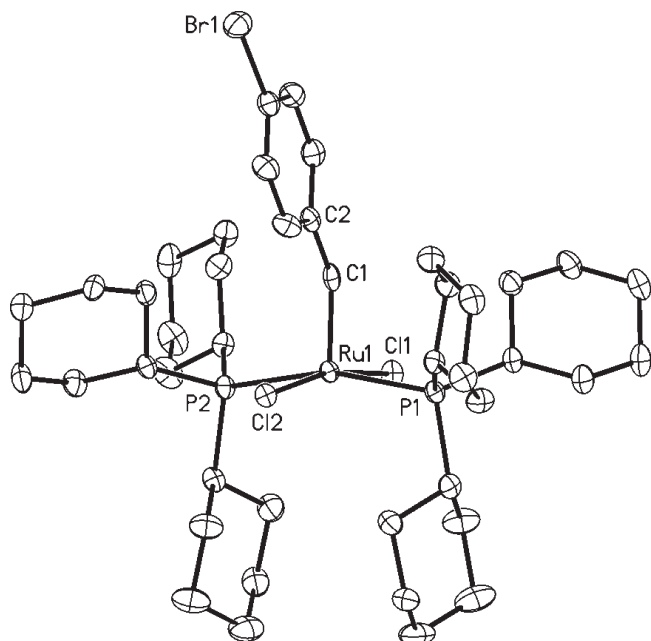
Figure 4. X-ray crystal structure of Grubbs first-generation *para*-bromobenzylidene complex. The bromine atom is remote from other ligands.

Table 3. Experimental Equilibrium Constants and Free Energies (Relative to Benzylidene) for Carbene Exchange of Aromatic Substrates

	X =	K_{eq} (mean, 10 trials)	ΔG (mean) (kcal/mol)
1	OCH_3	8.66(35)	−1.257(24)
2	CH_3		
3	Br	1.101(37)	−0.056(18)
4	Cl	1.248(43)	−0.129(20)
5	H	(1.000)	(0.000)
6	CO_2CH_3	0.367(6)	0.584(9)
7	CO_2H	0.295(10)	0.684(20)
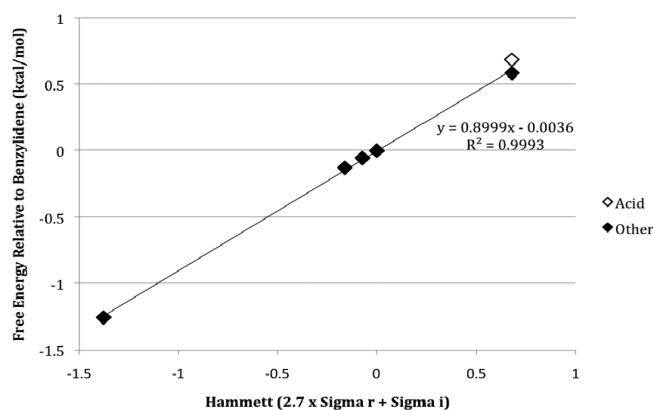
Figure 5. Gibbs free energy of *para*-substituted first-generation benzylidenes with respect to the parent vs a linear combination of Hammett σ_r and σ_i parameters. $\Delta G = 0.90$ kcal/mol (2.70 σ_r + σ_i) − 0.0036 kcal/mol, $R^2 = 0.9993$.

Since the ρ parameters are weighting factors, it is the proportion ρ_r/ρ_i that is important rather than the specific values of the individual parameters. We anticipated that inductive effects of the substituents would be fairly constant regardless of the reaction, while the resonance effects would
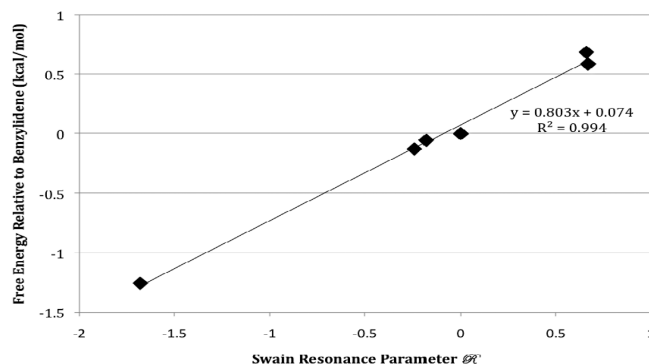
Figure 6. Gibbs free energy of *para*-substituted benzylidenes relative to the parent with respect to the Swain $\mathscr{R}$ parameter. ΔG (kcal/mol) = $0.803\mathscr{R} + 0.0744$, $R^2 = 0.994$.

be influenced to a large extent by the resonance donor/acceptor properties of the remainder of the molecule. Thus we set ρ_i to unity and varied ρ_r. Using $\rho_r = 2.7$ we were able to achieve an excellent fit for all substituents except the carboxylic acid, giving a correlation coefficient (R^2) of 0.9993, as shown in Figure 5. The large value of ρ_r with respect to ρ_i indicates that the free energy of the complexes is mainly a function of the resonance properties of the substituent rather than of inductive effects. This is emphasized by the fact that an excellent fit for all substituents, again with the exception of the carboxylic acid, with a correlation coefficient of 0.997, was also obtained by use of the Swain[15,16] resonance parameter $\mathscr{R}$ alone, without any contribution from the field parameter $\mathscr{F}$. As in the dual parameter correlation above, the carboxylic acid was somewhat above the trend line. When this data point was included, the correlation coefficient dropped slightly to 0.994 (Figure 6).

Our experimental data revealed that the ^{31}P and carbene ^{1}H chemical shifts varied with the substituent in the expected manner, electron-donating substituents giving upfield shifts, electron-withdrawing substituents giving downfield shifts. Interestingly, we found excellent linear free energy correlations of the ^{31}P shift by use of both the dual parameter method and Swain parameters, again with the exception of the carboxylic acid, which did not fit particularly well. The acid had a higher free energy and more downfield phosphorus shift than the ester even though Exner[14] gives identical σ_r° (Taft scale) and σ_i values for both of these groups. The published values[14] for the acid evidently are not appropriate to this system.

In contrast with the free energy and phosphorus shifts, the shift of the carbene protons did not correlate particularly well with the Hammett parameters of the substituents. Interestingly, however, we obtained an excellent fit, with a correlation coefficient of 0.997, by use of the *difference* between the shifts of the carbene and the corresponding internal alkene protons. A physical explanation of this observation is not obvious, but clearly [Ru]=CHAr and H_2C=CHAr place different electronic demands on the Ar substituent. The difference in ^{1}H shifts at CH reflects the degree to which replacement of CH_2 by [Ru] affects shielding at the CH, as modified by the degree to which Ar can exert a compensatory electronic effect. So we view this observation as at least qualitatively reasonable.
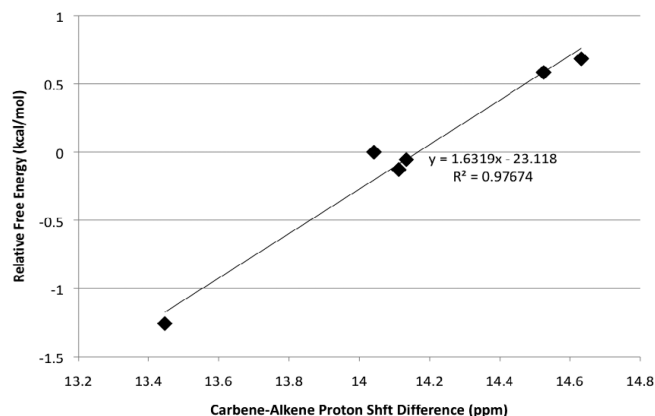
(15) Swain, C. G.; Lupton, E. C., Jr. *J. Am. Chem. Soc.* **1968**, *90*, 4328–4337.
(16) Swain, C. G.; Unger, S. H.; Rosenquist, N. R.; Swain, M. S. *J. Am. Chem. Soc.* **1983**, *105*, 492–502.
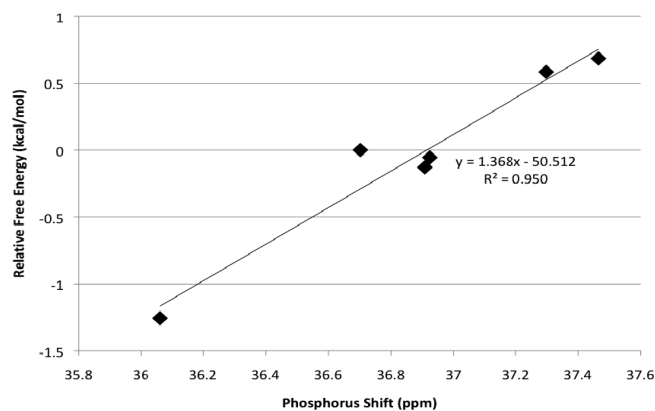
Figure 7. Free energy vs ^{31}P shift for *para*-substituted benzylidenes. Free energy (kcal/mol) = 1.368 kcal/mol·ppm − 50.512 kcal/mol.

Figure 8. Free energy vs carbene ^{1}H shift for *para*-substituted benzylidenes. Free energy (kcal/mol) = 1.632 kcal/mol·ppm − 23.112 kcal/mol.

In Figures 5 and 6 we demonstrated the correlation between linear free energy parameters and the experimentally measured relative Gibbs free energies of these complexes. Given the correlations between the free energy parameters and the NMR data described above, it seemed reasonable to see how well NMR data could be used as an indicator, in effect, a surrogate measure of the relative free energies of the complexes. Figures 7 and 8 demonstrate that, indeed, measured free energies of the ruthenium carbene complexes correlate rather well with both phosphorus shifts and (carbene − alkene) proton shift differences. The correlation coefficient using ^{31}P shifts (0.950) is not quite as good as that using the proton data (0.976), but both are good enough to be potentially useful. These figures display *purely experimental data*, and we note that the carboxylic acid is no longer an outlier. Instead, it is styrene itself that falls somewhat above both lines, reflecting slightly smaller chemical shifts for both the phosphorus and the carbene hydrogen than expected on the basis of the measured relative free energy.

The decrease in free energy of *para*-substituted benzylidenes with increasing electron-donating ability of the substituent is consistent with the electrophilic nature of the ruthenium atom in these complexes. The very high degree of correlation of the free energy with both the Hammett and Swain parameters confirms our expectation that substitution at this position exerts a purely electronic effect. While this could be expected to involve some combination of resonance and inductive effects, the fact that the ρ_r/ρ_i ratio is 2.70 in the

Table 4. Predicted Free Energies of *para*-X-Benzylidene Complexes (relative to X = H) Estimated from $\Delta G = 0.90\,(2.7\sigma_r(BA) + \sigma_i) - 0.0036$ kcal/mol

| X	$\sigma_r(BA)$	σ_i	predicted ΔG, kcal/mol	predicted K_{eq}
NHAc	0.36	0.26	1.232	0.121
NO$_2$	0.15	0.65	0.946	0.197
CN	0.13	0.56	0.816	0.246
COCH$_3$	0.16	0.28	0.637	0.335
I	−0.16	0.39	−0.0414	1.07
CH$_3$	−0.11	−0.04	−0.307	1.69
F	−0.45	0.5	−0.647	3.04
NMe$_2$	−0.83	0.06	−1.967	29.3

dual parameter analysis and that the variation is accounted for entirely by the Swain resonance parameter $\mathscr{R}$ points to the effect being largely, if not entirely, due to resonance with little if any contribution from field effects.

As mentioned earlier, we were not able to experimentally determine the free energy of the *para*-methyl complex since the ^{1}H NMR signals for the substrate partially overlapped those of styrene (Table 1). However, plotting the $\sigma_r(BA)$ and σ_i parameters of the methyl substituent against the ^{31}P chemical shift of the complex gives a point that fits well with the line correlating that data for the other substituted complexes. Thus we can proceed to *predict* the free energy and carbene exchange equilibrium constant of the *para*-methyl complex from either ^{31}P data or the Hammett parameters with some confidence. In Table 4 we use the latter to predict these thermodynamic parameters for several other *para*-substituted benzylidene complexes. In the systems whose free energies we were able to determine experimentally, the maximum deviation from the values estimated by our model was found to be 22.6 cal/mol (Figures 5 and 6). Since the standard deviation in each data set ranged from 9.4 to 23.5 cal/mol (Table 3), it seems reasonable to expect that our predicted free energies will approach the actual free energies of these complexes to a similar degree of accuracy.

X-ray Crystal Structures of Carbenes *trans*-(Cy$_3$P)$_2$Cl$_2$-Ru=CH(*p*-C$_6$H$_4$X), X = OCH$_3$, CH$_3$, Br, and H. As already mentioned, our NMR data are consistent with the *para* substituents in benzylidene carbene complexes exerting a purely electronic effect. Thus, as the donor atom contributes electron density to the electrophilic carbene carbon, the degree of back-bonding from the metal should decrease, and the less electron-deficient metal should in turn be less strongly bonded to phosphorus.

This model has clear structural implications. Depending upon the strength of the effect, electron donors should (a) decrease the carbene carbon−aromatic ring bond distance, (b) increase the metal−carbene bond distance, and (c) increase the metal−phosphorus bond distance.

To test this hypothesis, we crystallized several of the complexes and analyzed them by single-crystal X-ray diffraction. We were unable to crystallize the ester. The carboxylic acid gave a structure that was possibly twinned and did not refine well due to the presence of disordered solvent. The structure of the chloro derivative has been previously published.[4] The three catalyst derivatives, *trans*-(Cy$_3$P)$_2$Cl$_2$Ru=CH(*p*-C$_6$H$_4$X), X = OCH$_3$, CH$_3$, Br (Figure 4), are isostructural and crystallize in the triclinic crystal system. The parent compound, X = H, crystallizes in the monoclinic crystal system. All four structures were found to be benzene solvates. Crystal data are tabulated in the Experimental Section.
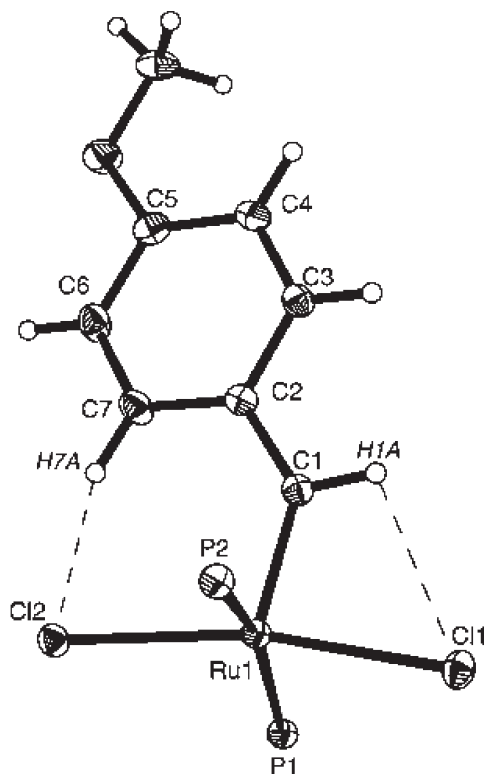
Figure 9. A portion of the crystal structure of *trans*-(Cy$_3$P)$_2$Cl$_2$Ru=CH(*p*-C$_6$H$_4$OCH$_3$) highlighting the intramolecular hydrogen-bonding interactions. Cyclohexyl groups on phosphorus are omitted for clarity.

Table 5. Hydrogen-Bonding Interactions in the Series of G1 Catalysts *trans*-(Cy$_3$P)$_2$Cl$_2$Ru=CH(*p*-C$_6$H$_4$X)

	X	C$\cdots$Cl (Å)	C-H$\cdots$Cl (Å)[a]	C-H$\cdots$Cl (deg)
1	OCH$_3$	2.993(2)	2.63	102.9
		3.288(2)	2.48	143.3
2	CH$_3$	2.975(3)	2.60	104.2
		3.330(4)	2.53	141.6
3	Br	2.971(3)	2.60	103.7
		3.318(4)	2.52	141.6
4	Cl[b]	2.990	2.62	103.0
		3.307	2.50	142.1
5	H	2.956(3)	2.58	103.9
		3.344(3)	2.53	141.1

[a] All C−H distances are normalized to 0.96 Å. [b] Data from ref 4

The Ru complexes have distorted square-pyramidal geometry with the benzylidene as the axial ligand, similar to the nonsolvated *p*-Cl derivative. Two phosphorus atoms of tricyclohexylphosphines and two chlorides make up the square plane and are in a *trans* configuration. The average dihedral angle between the RuP$_2$ and RuCl$_2$ planes is 83.3(8)°. The ruthenium shows a consistent shift out of the square plane toward the benzylidene, with an average displacement of 0.309(2) Å. The benzylidene is nearly coplanar with the *trans* chlorides, with an average dihedral angle of 12.20(14)°. This coplanar arrangement creates opportunities for intramolecular chloride−hydrogen hydrogen-bonding interactions between C−H donors and Cl−Ru acceptors, which undoubtedly affect the orientation of the alkylidene with respect to the Cl−Ru−Cl plane. Figure 9 illustrates the two important interactions.

(17) Brammer, L.; Bruton, E. A.; Sherwood, P. *Cryst. Growth Des.* **2001**, *1*, 277–290.

Table 6. Selected Bond Distances (Å) in the Series of G1 Catalysts *trans*-(Cy$_3$P)$_2$Cl$_2$Ru=CH(*p*-C$_6$H$_4$X)

	X	Ru−Cl	Ru−P	Ru−C	Ar−C
1	OCH$_3$	2.3920(4)	2.4157(6)	1.8453(15)	1.462(2)
		2.3952(4)	2.4208(4)		
2	CH$_3$	2.3930(10)	2.4094(10)	1.824(4)	1.475(5)
		2.3903(9)	2.4195(10)		
3	Br	2.3925(8)	2.4127(8)	1.825(3)	1.478(4)
		2.3939(8)	2.4202(8)		
4	Cl[a]	2.401(1)	2.435(1)	1.839(3)	1.475(5)
		2.395(1)	2.397(1)		
5	H	2.3957(6)	2.4030(7)	1.841(2)	1.461(3)
		2.3949(6)	2.4066(7)		

[a] Data from ref 4.

Brammer et al. studied the occurrence and strengths of such interactions and found that they are nontrivial.[17] In these compounds, the bond lengths and angles suggest that the interaction between Cl2 and H7A, and to a lesser extent the Cl1 and H1A interaction, should be considered "weak donor, strong acceptor" systems and could have bond energies of 1 kcal/mol, similar to a weak hydrogen bond. For each compound, including the previously published structure with X = Cl, Table 5 gives the hydrogen-bonding interaction for H7A$\cdots$Cl2 followed by that of H1A$\cdots$Cl1.

The integrity of the 2-fold hydrogen-bonding interaction is likely preserved in the first mechanistic step, phosphine exchange. The lack of ^{31}P−^{1}H coupling strongly suggests that the solution geometries correspond to those in the solid state.

We were also interested in whether there was any correlation between the coordination geometry of Ru and the free energy. Bond distances surrounding Ru are reported in Table 6. As the data in Table 6 show, no general correlation is evident. Only the methoxy substituent appears to display the expected effect compared with the other entries, in particular a short C−Ar bond and a long Ru=C bond. It should be remembered that the range of free energies of the complexes examined was only 1.26 kcal/mol; thus crystal-packing forces are certainly capable of dominating the observed structures in the solid state.

Aliphatic Carbenes: Linear and Branched Alkylidenes. The results of the exchange experiments of a Grubbs first-generation catalyst with aliphatic alkenes are presented in Table 7. The linear alkylidenes having three or more carbons had virtually identical free energies (mean = 0.683 ± 0.036 kcal/mol), as shown in Figure 10. Not surprisingly, branched alkylidene complexes are higher in energy, no doubt mainly a consequence of increased steric congestion. We indeed find a fairly decent correlation between free energies and the ^{1}H NMR shifts of the carbene protons for alkylidene complexes unbranched at the carbon adjacent to the carbene carbon. Figure 11 shows this relationship for complexes derived from alkenes 8−15, 19, and 20 (a single point represents the mean of the nearly invariant values for the straight-chain systems 10−15). The carbene derived from allyltrimethylsilane is an outlier (open diamond), presumably owing to an electronic effect superimposed upon the steric interactions.

Although the correlation is not quite as clean, the ^{31}P signal shifts upfield with increasing steric bulk of the carbene alkyl substituent, the opposite behavior of that of the carbene ^{1}H signal. We can rationalize these effects by postulating that interaction with a bulky carbene substituent forces the phosphorus away from the metal center, decreasing electron donation from the phosphorus to the metal. The

Table 7. Experimental Equilibrium Constants and Free Energies (relative to benzylidene)

Substrate	K_{eq} (mean, 10 trials*)	ΔG (mean) (kcal/mol)
8	8.66(25)	−1.251(17)
9	1.76(11)	−0.326(37)
10 C_2	0.34(21)	0.624(36)
11 C_3	0.286(6)	0.729(12)
12 C_4	0.323(12)	0.660(21)
13 C_5	0.304(8)	0.694(15)
14 C_6	0.304(11)	0.695(21)
15 C_8	0.304(6)	0.694(12)
16	0.00188(11)	3.677(33)
19	0.128(8)	1.208(33)
20	0.0148(4)	2.469(14)
21 (ATMS)	0.0364(22)	1.932(36)
22 (DEAM)	0.172(4)	1.026(13)
23 (DEAMM)	0.00455(33)	3.143(42)
24 (DEAEM)	0.00210(12)	3.596(33)
25 (DEAPM)	0.00186(14)	3.787(42)

*9 trials for entry 13 and 24 trials for entry 8.

higher residual electron density on phosphorus leads to an upfield shift in the ^{31}P resonance. In turn, the lower electron density on the metal decreases its back-donation to the carbene, resulting in a downfield shift of this resonance.

The alkylidenes branched in the 2 position do not appear to follow this trend. The free energy of the 2-methylpropylidene complex (entry 16) is approximately 3.1 kcal/mol higher than the NMR correlation of Figure 10 would suggest. The free energies of the 2,2-dimethylpropylidene and 2-methylbutylidene could not be determined due to the very small K_{eq} for the exchange reactions, preventing
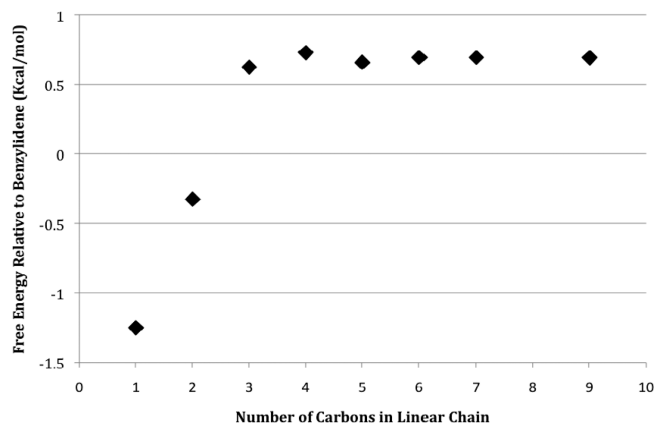
Figure 10. Gibbs free energy of linear alkylidenes of varying chain length.
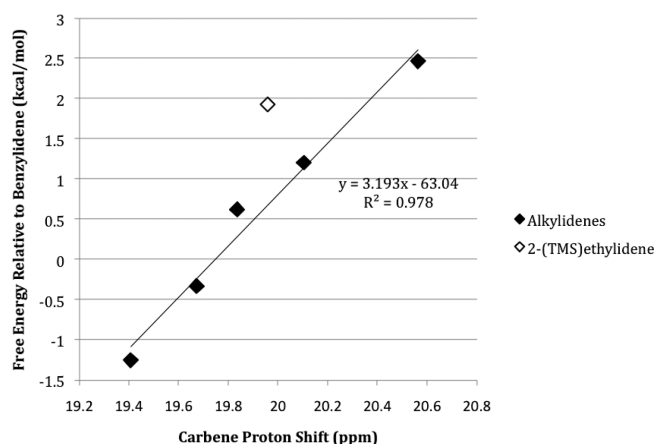
Figure 11. Free energy vs carbene proton shift (^1H_c) for alkylidene complexes not branched at carbon 2.

accurate integration of the alkylidene proton signal. Grubbs has previously noted the unreactive nature of 3,3-dimethyl-1-butene with first-generation catalysts.[4]

We noted a possibly relevant peculiarity in the ^{1}H NMR spectrum of the 2-methylpropylidene complex: While the coupling constants between the carbene hydrogen and the neighboring hydrogens in all other alkylidene complexes were similar to those in the corresponding alkenes, in this case *J* was substantially higher, 10.2 Hz in the carbene vs 6.6 Hz in the alkene. Together with the observation of only a single phosphorus resonance for this complex, this anomaly suggests that the carbene proton and adjacent methine proton have an *anti* relationship. If this were to be the case, then the terminal methyl groups on the alkylidene would lie on an axis parallel or nearly parallel with that of the phosphorus−metal bonds. In this conformation they would project between the cyclohexyl groups on the phosphine ligands and increase the free energy of the complex by inhibiting the rotation of the phosphorus ligands around the phosphorus−metal bonds.

The four allyl malonate ester complexes similarly show a significant increase in free energy and a concomitant decrease in K_{eq} as steric bulk increases. An anisotropic effect of the ester functional groups[18] on the phosphorus resonances

(18) Silverstein, R. M.; Webster, F. X.; Kiemle, D. J. *Spectrometric Identification of Organic Compounds*, 7th ed.; John Wiley & Sons: New York, 2005.

Table 8. Crystal Data and Data Collection Parameters for the Structures of *trans*-(Cy$_3$P)$_2$Cl$_2$Ru=CH(*p*-C$_6$H$_4$X)·*n*C$_6$H$_6$

	X =			
	OCH$_3$	CH$_3$	Br	H
formula	C$_{50}$H$_{80}$OP$_2$Cl$_2$Ru	C$_{50}$H$_{80}$P$_2$Cl$_2$Ru	C$_{49}$H$_{77}$P$_2$Cl$_2$BrRu	C$_{52}$H$_{81}$P$_2$Cl$_2$Ru
fw	931.05	915.05	979.93	940.08
T, K	90(2)	90(2)	90(2)	90(2)
λ, Å	0.71073	0.71073	0.71073	0.71073
cryst syst	triclinic	triclinic	triclinic	monoclinic
space group	*P*$\bar{1}$	*P*$\bar{1}$	*P*$\bar{1}$	*P*2$_1$/*n*
a, Å	9.8000(5)	9.8594(18)	9.8233(6)	9.6923(3)
b, Å	12.5772(7)	12.668(2)	12.6850(8)	13.4885(5)
c, Å	21.3245(12)	20.874(4)	20.9842(12)	37.6549(13)
α, deg	73.722(2)	74.289(2)	74.320(2)	90
β, deg	80.803(2)	80.083(2)	80.179(2)	92.559(2)
γ, deg	69.403(2)	68.871(2)	69.200(2)	90
V, Å^3	2356.3(2)	2332.9(7)	2345.3(2)	4917.9(3)
Z	2	2	2	4
cryst size, mm^3	0.44 × 0.21 × 0.15	0.69 × 0.11 × 0.11	0.25 × 0.09 × 0.07	0.22 × 0.18 × 0.10
rflns coll	33 887	24 443	28 758	69 823
	12 633	8540	10 073	13 235
indep rflns	[*R*$_{int}$ = 0.0291]	[*R*$_{int}$ = 0.0546]	[*R*$_{int}$ = 0.0557]	[*R*$_{int}$ = 0.0632]
data/restraints/params	12 633/0/506	8540/0/497	10 073/0/496	13 235/0/489
GOF on *F*^{2}	1.049	1.015	1.014	1.05
R$_1$ [*I* > 2*σ*(*I*)]	0.0287	0.0457	0.0390	0.0419
wR$_2$ [*I* > 2*σ*(*I*)]	0.0676	0.1013	0.0786	0.0963
R$_1$ (all data)	0.0349	0.0661	0.0679	0.0604
wR$_2$ (all data)	0.0705	0.1088	0.0881	0.1041
largest diff peak and hole, e Å^{-3}	0.510/−0.326	0.848/−0.794	0.510/−0.805	0.662/−0.772

of the malonate esters was quite noticeable, relative to the simple alkylidene complexes. Nevertheless, the trend for more upfield shifts of the ^{31}P resonance as free energy increases is quite evident (Tables 2 and 5).

Conclusions

A practical method for determining the relative thermodynamic stabilities of Grubbs first-generation carbene olefin metathesis catalysts has been developed. Equilibration between the benzylidene carbene and the carbene formed from its reactions with added alkenes occurs within minutes. Equilibrium constants may be readily obtained by means of ^{1}H NMR spectroscopy, thus complementing the extensive kinetic work published by the Grubbs group. These experimental data are consistent with and correlate well with published substituent parameters for both aromatic and aliphatic systems. In addition, NMR data show sensitivity to the same features that affect stability, enabling predictive correlations to be drawn involving systems for which direct measurement of relative energy is not possible.

Experimental Section

General Procedures. Grubbs first-generation catalyst was purchased commercially (Aldrich) and used as received. Grubbs first-generation methylidene complex was synthesized according to the literature procedure.[4] Dichloromethane was distilled from P$_2$O$_5$; THF was distilled from sodium benzophenone ketyl, both under dry N$_2$. Benzene, deuterated benzene, and pentane were dried over type 3 Å molecular sieves for at least 24 h followed by at least three freeze−pump−thaw cycles. C$_6$D$_6$ for NMR use was spiked with a small, unmeasured amount of tetramethylsilane. All manipulations of air-sensitive compounds were carried out on a Schlenk line under argon or in a Vacuum Atmospheres glovebox under N$_2$. All substrates were obtained commercially and used as received with the exception

(19) (a) Bhide, B. V.; Sudborough, J. J. *Chem. Zentr.* **1926**, *I*, 81. (b) Hjelt, E. *Chem. Ber.* **1896**, *29*, 1855–1859.

of the three diethyl allyl(alkyl)malonates, which were synthesized by alkylation of diethyl allylmalonate in accordance with literature procedures.[19] Infrared spectra were obtained neat using a Mattson Genesis II spectrometer equipped with a Graseby Golden Gate solid sampling accessory. NMR spectra of compounds were obtained in C$_6$D$_6$ on Varian Mercury Plus 300 FT-NMR, Varian Inova 400 FT-NMR, and Varian VNMRS 600 MHz FT-NMR spectrometers.

General Procedures for Equilibration Experiments. In order to acquire accurate NMR integration data, D2 was chosen to be at least 5 times the longest T_1 relaxation time of the signals under observation. The T_1 times for the carbene protons in the benzylidene, methylidene, and representative alkylidene complexes in C$_6$D$_6$ are all on the order of 0.35 to 0.5 s. The T_1 values for the corresponding alkene and styrene protons are much longer, on the order of 4.5−5 s. Thus a D2 of 25 s was used for studies of equilibration of benzylidenes and alkylidenes. The protons of ethylene have a T_1 of 8 s; thus a D2 of 40 s was used when studying equilibrations involving this substrate. In the glovebox a 0.5 mL aliquot of a stock solution of 0.26 mM Grubbs first-generation catalyst in C$_6$D$_6$ (stored frozen when not in use) was placed in a 5 mm diameter NMR tube, and the tube sealed with a neoprene rubber septum. The sample was removed from the glovebox and the septum sealed to the tube with electrical tape. Liquid substrates were added to the catalyst solution via syringe. The usual volume of substrate was 10 μL. In the case of substrates known to have unfavorable equilibrium constants, a larger volume of substrate was used, ranging from 14 to 20 μL, as appropriate. Solid substrates (*p*-vinylbenzoic acid and methyl *p*-vinylbenzoate) were added to the NMR tube in the glovebox prior to introduction of the catalyst solution. Gaseous substrates (propene, 1-butene, and 3-methyl-1-butene) were introduced as follows. The NMR tube was chilled in an ice-salt bath. Once the solvent was frozen, the atmosphere over the sample was removed with a high-vacuum pump through a syringe needle, and one atmosphere of the substrate gas introduced. The sample tube was then warmed to room temperature and shaken to dissolve the substrate gas in the reaction solvent.

All samples were allowed to equilibrate at room temperature (20−21 °C) prior to taking data. Samples containing liquid aliphatic hydrocarbon substrates were allowed to equilibrate for at least one hour. Samples containing liquid aliphatic ester

substrates were allowed to equilibrate for 1 to 3 h. Aromatic substrates were allowed to equilibrate for 24 to 27 h. In the case of the sample containing propene, the sample was allowed to equilibrate for four days prior to taking data. In the case of 1-butene, the equilibration time was shortened to one hour since the substrate underwent substantially more complete conversion overnight and the shorter equilibration time proved adequate. Samples containing ethylene were generated by allowing the samples containing linear aliphatic C_5, C_6, C_8, and C_{10} substrates to stand at rt for five days.

Proton NMR spectroscopy was used to collect data for equilibrium determination as follows. Proton spectra of samples containing aromatic substrates were recorded at 600 MHz. Proton spectra of samples containing aliphatic substrates were recorded at 400 MHz with the exception of the sample containing 4,4-dimethyl-1-pentene, in which case data were collected at 600 MHz. Phosphorus spectra for all samples were collected using the 300 MHz instrument operating at 121 MHz.

The interpulse delay interval, D2, was set to 25 s for all samples except ethylene. The delay for samples containing ethylene was set to 40 s. A tip angle of 45° was used. Eight scans were averaged for each spectrum. Ten spectra were obtained for each sample with the exception of that containing 1-heptene, for which only nine spectra were obtained. Six spectra were obtained for each of the samples containing ethylene. The equilibrium constants for the carbene exchange reactions were determined for each spectrum by multiplying the ratio of the integrals of the alkylidene to benzylidene protons by the ratio of the internal alkene protons of styrene to substrate. The equilibrium constants for each substrate were averaged, and the mean and standard deviation reported. The equilibrium constant for each spectrum was used to calculate the ΔG of the exchange reaction by employing the relation $\Delta G = -RT \ln(K_{eq}) = -1.987 \ln(K_{eq})$. The ΔG values for each substrate were averaged, and the mean and standard deviation are reported.

Synthesis of Diethyl Allyl(propyl)malonate [representative alkylation procedure].[19] A solution of 26 mmol of NaOEt in 50 mL of anhydrous ethanol was treated with 5.01 g (25.0 mmol) of diethyl allylmalonate under dry air and stirred for 2 h. The reaction mixture was treated with 4.02 g (32.7 mmol; 26% excess) of *n*-propyl bromide, and the mixture stirred overnight. After solvent evaporation the residue was taken up in hexane, the solids removed by filtration, and the filtrate stripped. The resulting oil was filtered through silica gel with 9:1 hexane/ethyl acetate as mobile phase and the eluent removed *in vacuo* to give an oil weighing 3.79 g, which contained 16% starting diester by ^{1}H NMR spectroscopy. This mixture was realkylated as above

with 7.8 mmol of NaOEt and 13.2 mmol of *n*-propyl bromide. After running the resulting crude product through a silica plug and removing solvent as above, 3.00 g (50% yield) of the desired product was obtained as a colorless oil. ^{1}H NMR indicated at least 95% purity. IR: 3077, 1728, 1646 cm^{-1}. ^{1}H NMR (300 MHz, C_6D_6): δ 0.84 (t, $J = 6$ Hz, 3H), 0.95 (t, $J = 6$ Hz, 6H), 1.29 (mult, 2H), 2.04 (mult, 2H), 2.83 (t, $J = 8$ Hz, 2H), 3.99 (q, $J = 7$ Hz, 4H), 5.01 (d, $J = 2$ Hz, 1H), 5.76 (mult, 1H). ^{13}C NMR: δ 13.9, 14.4, 17.5, 34.8, 37.4, 57.5, 60.7, 118.4, 133.2, 170.9.

Crystallization of Benzylidene Complexes. A mixture of 134 mg of Grubbs first-generation catalyst was warmed gently with 0.8 mL of benzene in a sealed vial. Crystals suitable for X-ray diffraction analysis were obtained by allowing the mixture to cool slowly to rt.

For the substituted systems, four solutions of 55 mg of Grubbs first-generation catalyst in 2 mL of benzene were treated, respectively, with 100 μL of *para*-chloro-, bromo-, methoxy-, and methylstyrenes. The chloro and bromo complexes crystallized on standing at rt overnight. The methoxy and methyl complexes crystallized on standing at rt for four days.

X-ray Crystal Structure Determinations. Crystals of *trans*-$(Cy_3P)_2Cl_2Ru$=$CH(p\text{-}C_6H_4X)\cdot C_6H_6$ (X = OCH_3, CH_3, Br, H) were mounted in the 90(2) K nitrogen cold stream provided by a CRYO Industries low-temperature apparatus on the goniometer head of a Bruker SMART Apex II diffractometer. Diffraction data were collected with graphite-monochromated Mo Kα radiation employing 0.3° ω scans and approximately a full sphere of data to $2\theta_{max}$ of 50.5° to 60°. A multiscan correction for absorption was applied using the program SADABS. The structures were solved by Patterson methods (SHELXS97) and refined by full-matrix least-squares on F^2 (SHELXL97).[20] All non-hydrogen atoms were refined with anisotropic thermal parameters. The H atoms on C atoms were generated geometrically and refined as riding atoms with C–H = 0.95–0.99 Å and $U_{iso}(H) = 1.2$ times $U_{eq}(C)$ for CH, CH_2. Crystal data and data collection parameters are given in Table 8.

Supporting Information Available: Tables of crystal data, atomic coordinates, and experimental details for the reported crystal structures are available in cif format. Figures of the crystal structures are also available. This material is available free of charge via the Internet at http://pubs.acs.org.

(20) Sheldrick, G. M. *Acta Crystallogr. A* **2008**, *64*, 112–122.